A Comparative Assessment of Deformation Behaviour and Weld-Zone Hardness in 4130 Cr–Mo and Dual-Phase Steel Tube

Jared Knapp[1]
[1] Industrial Tube Manufacturing, Hamilton, New Zealand

Corresponding author:
jared.knapp@industrialtube.co.nz

Publication date: August 2026

Abstract

The structural performance of welded tube assemblies is commonly evaluated using bulk material properties such as yield strength and ultimate tensile strength. Although these metrics are important, they do not fully describe post-yield deformation or the local mechanical conditions created by welded-joint geometry and heat-affected-zone variation.

This study compares seamless AISI 4130 chromium–molybdenum steel tube supplied in the normalised condition (Condition N in accordance with AMS6360R), hereafter referred to as 4130 Cr–Mo, with UltraTube RS, a dual-phase steel tube manufactured by cold forming and high-frequency induction welding. Test specimens were closely matched in mechanical strength and section profile to minimise the influence of nominal strength and geometry.

The investigation combined tensile testing, weld-zone microhardness profiling, finite element analysis, fabrication observations and comparative tube-level deformation testing. The materials exhibited closely comparable proof and ultimate tensile strengths, while UltraTube RS showed a lower yield ratio, greater elongation and more distributed tensile deformation before final localisation. TIG-welded 4130 Cr–Mo developed a pronounced local heat-affected-zone hardness peak of approximately 490 HV, compared with a lower peak of approximately 312 HV and a more gradual hardness transition in UltraTube RS. Finite element analysis identified the branch-to-main-tube interface as the principal region of geometric stress demand for both materials.

Both materials were successfully welded and accommodated the applied bending and flattening conditions. The clearest difference was observed during axial compressive collapse, where UltraTube RS developed broader, more progressive folding, while 4130 Cr–Mo developed sharper localised folds and visible tearing. The results demonstrate that materials with comparable tensile strength can exhibit different post-yield responses and weld-zone property distributions, which are relevant to the development of localised deformation in welded tube structures.

1. Introduction

In welded tubular structures for motorsport, transport, and high-performance applications, failure is rarely governed by tensile overload. Instead, structural integrity is determined by localised conditions, including stress concentrations at weld toes, geometric discontinuities, and microstructural variation within the heat-affected zone (HAZ).

4130 Cr–Mo steel has been one of the benchmark materials in these applications due to its high strength-to-weight ratio and established fabrication practices. However, advances in steel metallurgy have led to the development of advanced high-strength steels (AHSS), including dual-phase grades that achieve comparable strength through fundamentally different microstructural mechanisms (Fonstein, 2015). This broader shift reflects the direction of modern automotive structural engineering, which moved away from traditional alloy-steel strengthening philosophies decades ago in favour of material systems engineered around controlled deformation behaviour, crash-energy management, manufacturability, and structural efficiency.

Dual-phase steels have been widely adopted in automotive body-in-white structures (WorldAutoSteel, 2025) due to their ability to combine high strength with controlled, progressive deformation under crash loading conditions. This behaviour is achieved through microstructural engineering rather than alloy composition alone and is closely linked to strain hardening and deformation stability.

This study examines whether these differing material-design approaches produce measurable differences in deformation behaviour and weld-zone hardness in tubes with broadly comparable tensile properties and geometry.

2. Materials and Manufacturing Routes

2.1 Seamless 4130 Cr–Mo Tube Production

As illustrated in Fig. 1, seamless 4130 Cr–Mo tube is typically produced from continuously cast billet, which is reheated and subjected to rotary piercing, commonly by the Mannesmann process, to form a hollow shell. The shell is subsequently elongated and reduced by hot-working processes such as mandrel rolling or stretch reducing, with cold pilgering or cold drawing employed where required to achieve the final dimensions, tolerances, and surface finish (ASM International, 1998; Dieter, 1986).

The 4130 Cr–Mo tube examined in this study was supplied in the normalised condition, as stated on the manufacturer's material test report. Normalising typically produces a predominantly ferrite–pearlite microstructure, with mechanical properties governed primarily by alloy composition and heat-treatment history rather than by a deliberately engineered multiphase architecture (Bhadeshia & Honeycombe, 2017). Although some microstructural variation may arise from segregation, prior processing, or local cooling conditions, the material does not exhibit the intentionally controlled phase distribution characteristic of advanced high-strength steels.

Unlike dual-phase steels, this microstructure is not designed to actively partition strain between phases under load but instead exhibits a more uniform mechanical response at the macroscopic scale.

2.2 Dual-Phase Steel Production and HFIW Tube Manufacturing

Dual-phase steels are produced through tightly controlled thermomechanical processing, most commonly via continuous annealing lines. In this process, cold-rolled strip is heated into the intercritical region, where ferrite and austenite coexist, and is then rapidly cooled to form a microstructure consisting of a ferrite matrix with dispersed martensite islands (Fonstein, 2015; Bhadeshia & Honeycombe, 2017).

ArcelorMittal describes dual-phase steels as exhibiting low yield-to-tensile strength ratios, high initial strain-hardening rates, and the absence of yield point elongation, all of which contribute to stable plastic deformation under load (ArcelorMittal, 2025).

The processed strip is subsequently formed into tube via roll forming and joined using high-frequency induction welding (HFIW), producing a solid-state metallurgical bond formed under pressure. The tube forming process is designed to preserve the mechanical properties established during strip processing while introducing a degree of cold work.

Comparison of manufacturer mill certificates for the incoming strip, and the finished tube indicates an increase in strength following tube manufacture, consistent with the effects of strain hardening

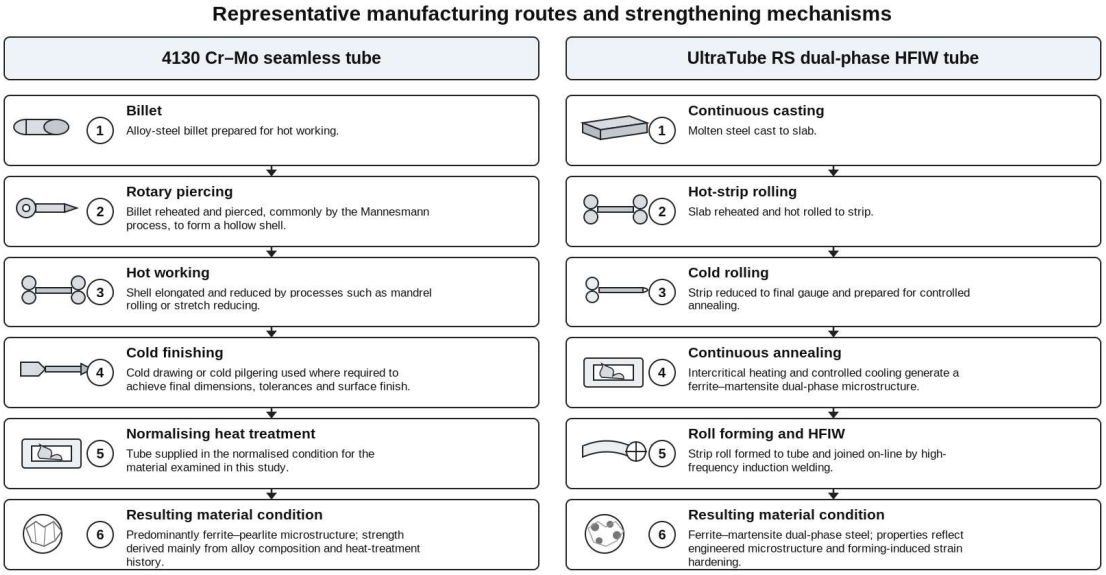

Fig. 1. Schematic comparison of manufacturing routes and strengthening mechanisms for seamless 4130 Cr–Mo tube and dual-phase HFIW tube.

associated with the cold-forming process (Fonstein, 2015). Accordingly, the final tube properties reflect both the engineered dual-phase microstructure established during continuous annealing and the effects of subsequent forming.

2.3 Comparison of Material Design and Strengthening Mechanisms

The distinction between these materials lies in how their mechanical properties are generated. Normalised 4130 Cr–Mo derives its behaviour from a combination of alloy composition and section heat treatment. Its strength is developed through conventional alloy-steel mechanisms, including solid-solution effects from alloying additions, carbon-dependent microstructural strengthening, grain-size effects, and the microstructural condition established during normalising. Chromium and molybdenum also increase hardenability, influencing the material's response to subsequent thermal cycles such as welding (Bhadeshia & Honeycombe, 2017; Kou, 2003; ASM International, 2011).

In contrast, dual-phase steel is deliberately engineered at the microstructural level, with its mechanical behaviour controlled through the interaction between a ferrite matrix and dispersed martensite islands.

These manufacturing approaches are fundamentally different in practice. The continuous annealing processes used to produce dual-phase microstructures are typically applied to flat-rolled strip under tightly controlled, continuous processing conditions, most commonly within high-volume automotive supply chains. In contrast, seamless tube production routes for alloy steels such as 4130 rely on alloy composition and subsequent heat treatment of the hollow section.

As a result, the mechanisms used to generate strength and control deformation behaviour in each material system are not directly interchangeable within conventional manufacturing routes. Normalised 4130 Cr–Mo relies on the combined effects of conventional alloying, microstructural transformation and heat treatment, whereas UltraTube RS derives its characteristic response from a deliberately engineered multiphase microstructure together with the effects of cold forming during tube manufacture.

Table 1. Chemical composition of tested materials (wt.%) derived from manufacturer material test certificates.

Material	C (wt.%)	Mn (wt.%)	Si (wt.%)	Cr (wt.%)	Mo (wt.%)
Seamless 4130 Cr–Mo tube	0.31	0.5	0.27	0.87	0.17
UltraTube RS dual-phase steel tube	0.09	1.9	0.25	0.21	0

3. Mechanical Properties and Deformation Behaviour

3.1 Tensile Behaviour

Longitudinal test pieces prepared from each tube were subjected to tensile testing in accordance with AS 1391:2020 (equivalent to ISO 6892-1). The measured 0.2% proof strengths and ultimate tensile strengths were closely comparable.

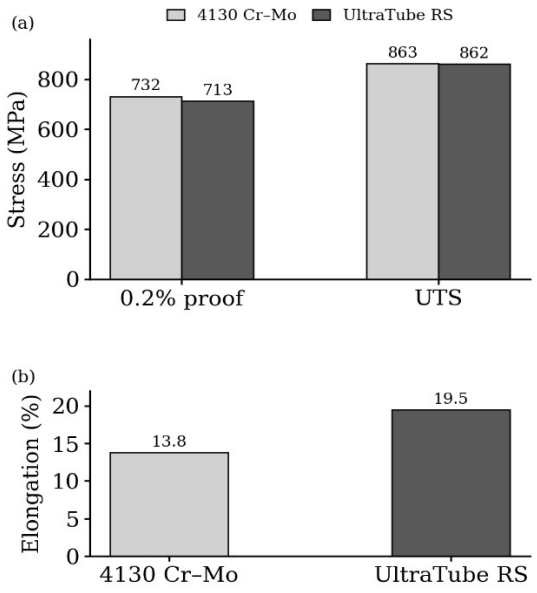

Fig. 2. Comparison of tensile properties of 4130 Cr–Mo and UltraTube RS specimens: (a) 0.2% proof strength and ultimate tensile strength; and (b) elongation to fracture.

The closely comparable proof and ultimate tensile strengths indicate that differences in subsequent deformation behaviour are unlikely to result from differences in nominal strength. Instead, the observed response is consistent with differences in post-yield strain accommodation and strain-hardening behaviour. In dual-phase steels, sustained strain hardening is commonly associated with a lower yield ratio and a higher strain-hardening exponent, n, which can delay strain localisation as plastic deformation develops.

Complete laboratory reports are provided in Appendix B (Materials & Testing Laboratories, 2026c, 2026d).

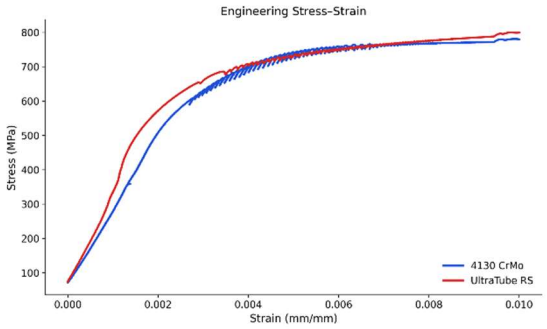

Fig. 3. Engineering stress–strain response of UltraTube RS and 4130 Cr–Mo. Despite near-identical ultimate tensile strength, UltraTube RS exhibits a lower yield-to-tensile strength ratio and higher effective strain-hardening capacity over the measured strain range, while 4130 Cr–Mo shows a higher yield ratio and earlier strain localisation

3.2 Specimen Strength and Section Equivalence

The two materials were selected before testing on the basis that their nominal tensile strength and tube geometry were broadly comparable. The intention was not to obtain exact equivalence but to minimise differences in initial strength and section properties that could otherwise dominate the comparison. The laboratory results presented in Section 3.1 subsequently confirmed that the materials had closely comparable proof and ultimate tensile strengths.

The longitudinal tensile specimens were also closely matched in cross-sectional dimensions and were tested using the same 50 mm gauge length. The 4130 Cr–Mo specimen measured 1.65 × 12.50 mm and had a cross-sectional area of 20.6 mm², while the UltraTube RS specimen measured 1.61 × 12.51 mm and had a cross-sectional area of 20.1 mm². The difference in specimen width was less than 0.1%, while the differences in thickness and cross-sectional area were approximately 2.4%.

Young's modulus was not separately determined in this study. However, the elastic modulus of steel is generally approximately 200-210 GPa and varies comparatively little between conventional and advanced high-strength steel grades (WorldAutoSteel, 2025). Elastic stiffness was therefore not treated as a principal differentiating variable. The comparison instead focused on behaviour after yielding, including strain hardening, deformation distribution and strain localisation.

Taken together, the prospective material selection, subsequent strength measurements and close dimensional alignment reduce the likelihood that the observed differences arose primarily from initial strength or specimen geometry. They provide a consistent basis for interpreting the differing tensile responses principally in relation to the materials' post-yield behaviour, subject to the limitations discussed in Section 9.

Fig. 4. Comparative tensile specimens before fracture (left) and after fracture (right). The UltraTube RS specimen (silver) exhibited greater distributed plastic deformation and necking prior to failure, whereas the 4130 Cr–Mo specimen (black) exhibited more localised deformation within the reduced section under the tested conditions.

3.3 Limitations of Elongation as a Deformation Metric

Elongation after fracture is commonly reported as an indicator of ductility; however, it is not a direct measure of strain distribution during deformation. The measured value is influenced by test-piece geometry, gauge length, the onset and extent of necking, and post-necking deformation. It should therefore be interpreted alongside the engineering stress–strain response and observed deformation morphology rather than as a standalone measure of structural deformation behaviour (Huda, 2024).

A distinction must also be made between uniform elongation, which describes deformation up to the point of maximum engineering stress, and total elongation, which includes the subsequent contribution of localised necking. Total elongation can therefore be influenced substantially by post-instability deformation and does not, in isolation, describe how uniformly strain was distributed before localisation (Cao et al., 2015).

This limitation becomes particularly relevant for advanced high-strength steels (AHSS), where deformation behaviour differs fundamentally from that of conventional mild and alloy steels. SSAB notes that conventional tensile elongation

measurements may underrepresent the true forming and deformation capability of dual-phase steels because deformation occurs highly locally rather than uniformly over the full gauge length (SSAB, n.d.).

In welded tubular structures, deformation behaviour is governed not only by total strain capacity, but by how progressively plastic deformation can be accommodated under load. Materials with sustained strain hardening tend to distribute deformation over a larger volume prior to localisation, whereas materials with lower strain hardening capacity tend to concentrate strain more rapidly once yielding begins.

ArcelorMittal identifies that dual-phase steels derive their characteristic behaviour from high initial strain hardening, continuous yielding behaviour, and low yield-to-tensile strength ratios, enabling sustained plastic deformation prior to localisation (ArcelorMittal, 2025).

In the present study, UltraTube RS exhibits higher elongation than 4130 Cr–Mo. However, the significance of this difference lies not simply in total strain capacity, but in how strain is distributed and sustained during deformation. Because dual-phase steels accommodate deformation through progressive strain redistribution, conventional elongation measurements may underrepresent the extent of the behavioural difference between the materials, particularly in welded structures where geometric and metallurgical discontinuities can promote localised strain concentration.

3.4 Post-Yield Deformation and Strain Distribution

The tensile results show that 4130 Cr–Mo has a slightly higher yield ratio than UltraTube RS, indicating a smaller difference between the onset of yielding and ultimate tensile strength. This is consistent with reduced post-yield strain-hardening capacity and an earlier tendency toward strain localisation (ArcelorMittal, 2025; Huda, 2024).

In the present study, the lower yield ratio and higher elongation of UltraTube RS, considered alongside the observed deformation of the tensile specimen, suggest that plastic deformation was sustained over a greater portion of the reduced section before final localisation.

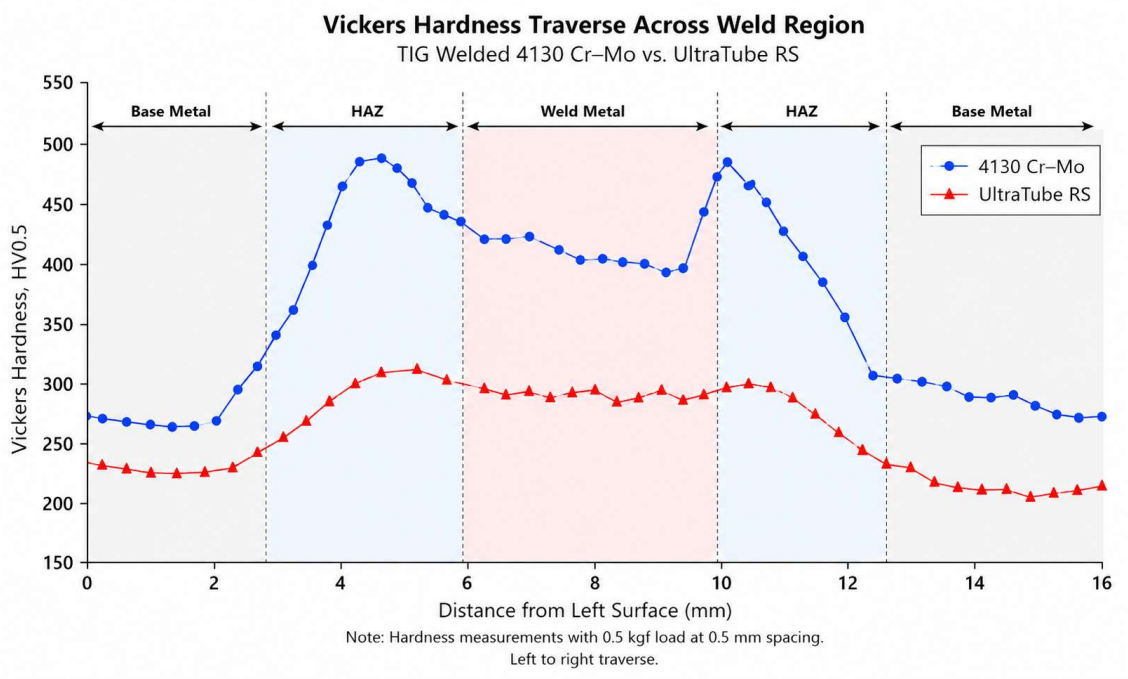

Fig. 5. Hardness profile based on 0.5 kg micro-Vickers traverse measurements at 0.5 mm spacing. Curves are an illustrative trend representative of discrete test data.

4. Weld Zone Behaviour and Hardness Distribution

Welding introduces localised thermal cycles that modify microstructure within both the weld metal and the adjacent heat-affected zone (HAZ), resulting in spatial variation in mechanical properties across the joint.

To quantify this effect, micro-Vickers hardness traverses were conducted by an independent laboratory (Materials & Testing Laboratories, Auckland) on TIG welded branch joints for both materials using a 0.5 kg load at 0.5 mm spacing (Materials & Testing Laboratories, 2026a, 2026b). Full datasets are provided in Appendix A.

4.1 4130 Cr–Mo Hardness Profile

The hardness profile for 4130 Cr–Mo exhibits a pronounced and highly localised peak within the HAZ. Base material hardness is typically in the range of approximately 266–306 HV, increasing sharply through the HAZ to a peak value of approximately 490 HV before reducing toward the weld metal and returning to base material levels.

This represents:

- an absolute increase of approximately 180–220 HV above the base material; and
- a steep hardness gradient occurring over a narrow spatial region of approximately 1–2 mm.

The observed hardness peak is consistent with transformation hardening caused by the local welding thermal cycle. Material close to the fusion boundary is heated above the austenitisation temperature and subsequently undergoes rapid self-quenching as heat is conducted into the surrounding tube.
The chromium and molybdenum additions in 4130 increase its hardenability, allowing the austenite to transform into hard martensitic and potentially bainitic constituents within the HAZ (Kou, 2003; ASM International, 2011). Metallographic phase identification would be required to confirm the precise microstructure responsible for the measured hardness peak.

4.2 UltraTube RS Hardness Profile

In contrast, UltraTube RS exhibits a significantly lower peak hardness and a more gradual transition across the weld region. Base material hardness is approximately 233–241 HV, increasing through the HAZ to a peak value of approximately 312 HV, before transitioning into weld metal values in the range of 285–306 HV (Materials & Testing Laboratories, 2026a, 2026b).

This represents:

- an absolute increase of approximately 70–80 HV above base material, and
- a broader, more distributed hardness transition across the HAZ and weld metal

---

4.3 Comparative Hardness Profiles

The distinction between the two materials is not limited to peak hardness but extends to the shape and gradient of the hardness profile across the weld region.

4130 Cr–Mo exhibits:

- a high peak hardness of approximately 490 HV;
- a steep hardness gradient between the base material and HAZ; and
- a pronounced localised hardness increase within the sampled HAZ.

UltraTube RS exhibits:

- a lower peak hardness of approximately 312 HV;
- a more gradual hardness transition; and
- lower variation in hardness across the sampled weld region.

A limited degree of HAZ softening in UltraTube RS may be advantageous in a welded node, as the resulting slightly softer and more ductile region avoids the pronounced local hardening and steep property gradient observed in the 4130 Cr–Mo specimen. From a fatigue perspective, the comparatively gradual hardness transition measured in UltraTube RS may be favourable, as lower HAZ hardness gradients have been associated with reduced fatigue damage and impeded crack propagation in welded dual-phase steel joints (Farabi et al., 2010; Lee et al., 2014; Xie et al., 2021).

4.4 Implications of Weld-Zone Hardness Variation

Increased hardness in steels is generally associated with reduced ductility and fracture toughness, increasing sensitivity to stress concentrations such as weld toes, defects and heat-affected-zone boundaries (Anderson, 2017; Dieter, 1986). Where a pronounced hardness peak occurs over a short distance, the resulting steep gradient creates an abrupt transition in local mechanical properties that can promote strain localisation under applied load.

The hardness profiles measured in this study provide a mechanistic explanation for the deformation behaviour discussed in later sections:

- The high, localised hardness peak in the 4130 Cr–Mo HAZ introduces a region of reduced ductility adjacent to comparatively softer material, creating a sharp mechanical transition through which strain may become concentrated.
- The lower peak hardness and more gradual hardness transition measured in UltraTube RS reduce the severity of this mechanical discontinuity, enabling deformation to be accommodated over a larger material volume (Materials & Testing Laboratories, 2026a, 2026b).

The limited HAZ softening observed in UltraTube RS may also be favourable from a fatigue perspective. Lower HAZ hardness gradients have been associated with reduced fatigue damage and impeded crack propagation in welded dual-phase steel joints (Xie et al., 2021). However, studies of welded dual-phase steels also demonstrate that fatigue behaviour depends on the degree and width of the softened region: mild, localised softening may have little adverse effect, whereas severe or broadly distributed softening can reduce fatigue resistance (Farabi et al., 2010; Lee et al., 2014).

The comparatively gradual hardness transition measured in UltraTube RS is therefore consistent with a more progressive local mechanical response and a reduced tendency for strain to become concentrated within a sharply hardened region. Fatigue performance was not measured directly in the present study, and this interpretation should therefore be regarded as an indication of potentially favourable weld-zone behaviour rather than direct evidence of improved fatigue life.

5. Finite Element Analysis of Welded Joint Response

The preceding tensile testing characterised the bulk mechanical response of the two materials, while the hardness traverses identified local variation across the welded regions. The physical deformation tests demonstrated how the tube sections behaved under severe loading. However, these methods do not directly identify where stress demand develops within an equivalent welded branch-joint geometry.

Finite element analysis was therefore undertaken to provide a joint-level link between the measured tensile behaviour and the deformation observed experimentally. Its purpose was to identify the location and distribution of stress within an equivalent welded joint and to examine how the differing tensile-derived material responses influenced the overall joint response when geometry and loading conditions were held constant.

A comparative finite element analysis was conducted by Kinetic Simulation using equivalent welded branch-joint geometries and loading conditions. Material models were derived from the experimentally measured stress–strain curves and incorporated multilinear isotropic hardening behaviour. The analysis therefore represented the measured yielding and post-yield response of each parent material rather than treating the two steels as having identical mechanical behaviour (Kinetic Simulation, 2026).

The equivalent-stress distributions shown in Figures 6 and 7 indicate that the highest stress demand occurred around the branch-to-main-tube interface for both materials. The concentration followed the welded joint profile, with the highest-stress regions developing near the intersection between the branch and main tube. The broadly similar location and overall pattern of stress concentration demonstrate that joint geometry is the primary factor determining where peak stress demand develops.

This result is significant because the materials were closely matched in tensile strength and section geometry. Comparable global strength did not remove the local stress concentration introduced by the branch-joint geometry. Instead, both material models developed their highest stress demand within the same general joint region, providing a common geometric basis on which their differing

material and weld-zone responses can be considered.

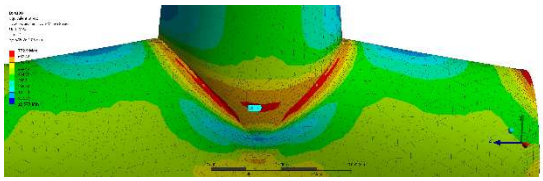

Fig. 6. Equivalent-stress distribution around the welded branch-joint region for normalised 4130 Cr–Mo.

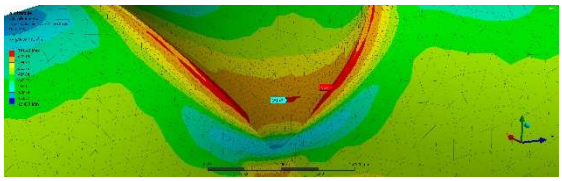

Fig. 7. Equivalent-stress distribution around the welded branch-joint region for UltraTube RS.

Figures 8 and 9 show the total-deformation distributions across the complete joint models. These plots provide broader context for the structural response by showing how displacement developed through the branch and main tube under the applied loading conditions. Total deformation should not, however, be interpreted as a direct measure of plastic-strain localisation or as evidence of crack initiation.

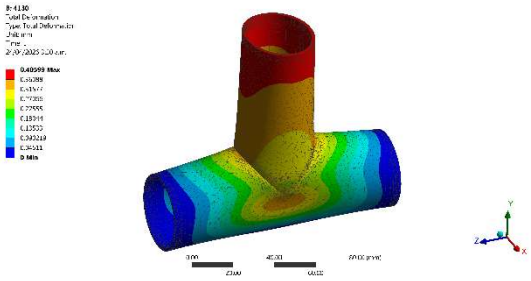

Fig. 8. Total-deformation distribution for the normalised 4130 Cr–Mo welded branch-joint model.

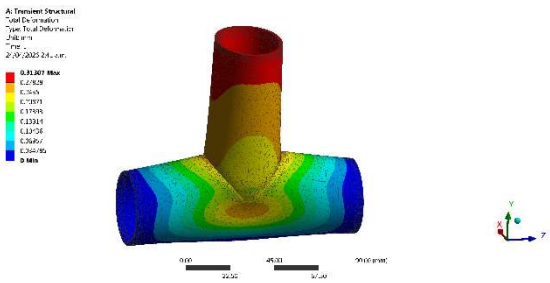

Fig. 9. Total-deformation distribution for the UltraTube RS welded branch-joint model.

The FEA therefore serves two specific functions within this study. First, it identifies the welded branch interface as the principal region of geometric stress concentration. Second, it provides a consistent joint-level framework within which the measured material response and weld-zone characteristics of the two steels can be interpreted.

The analysis did not incorporate a damage or fracture criterion and should not be interpreted as a direct prediction of crack initiation, fracture, fatigue life, weld-defect sensitivity, or progressive failure. Its contribution is to establish where geometric stress demand occurs and to provide the basis for considering how that demand interacts with the differing welded-node characteristics examined in the following section.

5.1 Interaction Between Joint Geometry and Weld-Zone Property Variation

The finite element analysis identified the branch-to-main-tube interface as the principal region of stress concentration for both material models. This establishes the location of greatest geometric demand within the joint but does not, by itself, represent the spatial variation in mechanical properties produced by welding.

The hardness traverses presented in Section 4 independently demonstrate that the two materials developed substantially different local property transitions across their welded regions. The 4130 Cr–Mo specimen exhibited a pronounced and relatively abrupt hardness increase adjacent to the weld, whereas UltraTube RS exhibited a lower and more gradual hardness transition. The relevance of these findings here is that the measured property variations occur within the same general joint region in which the FEA identifies the highest geometric stress demand.

Joint geometry and local mechanical-property variation perform distinct but interacting roles. In welded tubular joints, geometry and applied loading determine the location and distribution of stress concentration around the joint intersection and weld toe (Shao, 2007). Welded steel joints may also exhibit different local constitutive responses across the base material, heat-affected zone and weld metal, which can influence the distribution of deformation once yielding develops (Peng et al., 2018).

Based on the model description presented in this study, the hardness traverses were not incorporated as spatial material inputs to the finite element model. Instead, each material model was derived

from the corresponding parent-material stress–strain curve and represented using multilinear isotropic hardening. The analysis therefore identifies the region of geometric stress demand and compares the tensile-derived response of the two materials, but it does not directly calculate the effect of the measured weld-zone hardness gradients.

Taken together, the modelling and hardness results provide complementary evidence. In the welded 4130 Cr–Mo specimen, the principal region of geometric stress demand coincides with a comparatively abrupt measured hardness transition. In the UltraTube RS specimen, the same general geometric demand occurs alongside a lower and more gradual measured hardness transition.

The results suggest that the sharper weld-zone property transition in 4130 Cr–Mo may contribute to more localised deformation once yielding begins, whereas the more gradual transition in UltraTube RS is consistent with broader strain redistribution. This interpretation aligns with the physical test observations but was not directly represented in the present finite element model.

Within the scope of this study, the FEA establishes where stress demand is concentrated, while the hardness traverses characterise the differing local mechanical environments present within that region. This combined interpretation provides the basis for considering the fabrication and weld observations presented in the following section.

---

6. Comparative TIG Welding and Fabrication Observations

Comparative TIG welding trials were undertaken by an experienced motorsport fabricator under normal workshop conditions. The trials were intended to reflect the practical environment in which these materials are likely to be welded in motorsport applications.

Welding was performed using 1.6 mm ER70S-2 filler rod, non-pulsed TIG at fixed current, and argon shielding gas. The primary comparison comprised an UltraTube RS tee joint and a 4130 Cr–Mo tee joint, both welded at 77 A. An additional UltraTube RS joint was welded at 82 A to provide a qualitative visual comparison at a higher current setting.

As shown in Figure 10, the UltraTube RS and 4130 Cr–Mo joints welded at the common 77 A setting exhibited visibly different weld-zone appearances. The UltraTube RS joint showed a comparatively smooth and uniform visible fillet profile, while the 4130 Cr–Mo joint appeared to have a more pronounced central weld crown and a less uniform surface profile. The additional UltraTube RS joint welded at 82 A showed a broader region of visible thermal discolouration than the corresponding 77 A UltraTube RS joint.

Because the specimens differed in initial surface appearance and photographic orientation, these observations are qualitative and are not used to infer heat-affected-zone width or weld integrity. The 82 A specimen does not form part of the comparative hardness assessment.

Fig. 10. *TIG-welded tee joints produced under normal motorsport workshop conditions. The upper UltraTube RS specimen contains joints welded at 82 A on the left and 77 A on the right. The lower 4130 Cr–Mo specimen was welded at 77 A. The two 77 A joints provide the primary material comparison, while the 82 A UltraTube RS joint provides an additional qualitative comparison of weld-zone appearance.*

Macro examination of the two 77 A specimens reported satisfactory penetration and complete fusion, with no cracks, slag or porosity observed in either material (Materials & Testing Laboratories, 2026a; 2026b).

These 77 A specimens were subsequently used for the comparative hardness traverses presented in Section 4. The fabrication trials therefore establish that both materials were successfully welded into representative tee joints under comparable practical conditions, while the differing weld-zone hardness responses are presented and interpreted earlier in the study.

---

7. Physical Deformation Testing

The preceding sections examined tensile response, weld-zone hardness, and the response of fabricated branch joints. The focus now turns to tube-level deformation testing, in which the specimens were

assessed independently of the TIG-welded branch-joint geometry. This allowed the deformation characteristics of the tube sections themselves to be observed without the local geometric and mechanical-property variations introduced by a welded intersection.

Three-point bending, compressive collapse under a hydraulic press, rotary draw bending, and flattening were used to compare deformation morphology. Quantitative measurements are reported where available; otherwise, the comparison is based on observable differences in curvature distribution, fold formation, tearing, and cross-sectional distortion.

7.1 Three-point Bending Behaviour

Three-point bending was used to compare the deformation response of equivalent tube sections under transverse loading. Each specimen was supported between two cylindrical supports, with load applied through a central former. This arrangement generated the greatest bending demand at midspan while allowing the surrounding tube length to accommodate the imposed displacement through changes in curvature and cross-sectional geometry.

Both materials underwent substantial permanent deformation concentrated around the central loading region. No visible fracture was observed in either photographed specimen under the applied test conditions.

The test was qualitative, as load–displacement data and detailed measurements of the final bend geometry were not recorded. The results therefore demonstrate the ability of both materials to accommodate severe bending deformation but do not provide a quantitative basis for comparing bending strength, energy absorption or structural capacity.

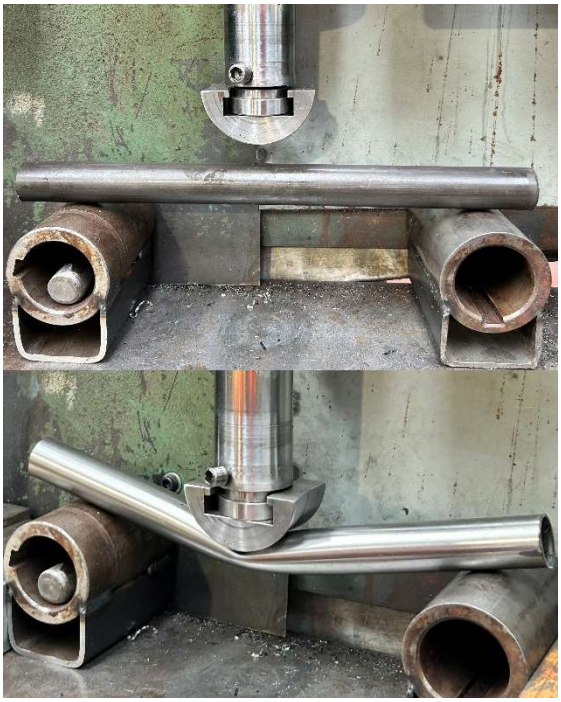

Fig. 11. Three-point bending arrangement used for the qualitative assessment: (a) tube specimen positioned across two cylindrical supports beneath the central loading former; and (b) specimen deforming as the former was displaced downward between the supports.

Fig. 12. Tube specimens following three-point bending. UltraTube RS is shown at the bottom and 4130 Cr–Mo at the top. Both underwent substantial permanent deformation without visible fracture.

7.2 Axial Compressive Collapse Behaviour

Short tube sections of equivalent nominal diameter, wall thickness and unsupported length were positioned vertically in an HPM-63T hydraulic press and loaded axially to produce progressive compressive collapse. Specimen dimensions were matched to minimise geometric effects on the observed deformation behaviour.

Fig. 13. Compressive-collapse testing using the 63T hydraulic press, showing a short tube specimen undergoing axial deformation beneath the loading platen.

Both materials underwent substantial plastic collapse; however, clear differences were observed in the resulting deformation morphology. UltraTube RS exhibited broader, more progressive folding distributed around the collapsed section. In contrast, the 4130 Cr–Mo specimen developed sharper and more localised folds.

Visible tearing occurred in the 4130 Cr–Mo specimen within a region of severe local deformation. No comparable tearing was observed in the UltraTube RS specimen under the applied loading condition, and no separation of its longitudinal production seam was observed. These observations are consistent with the post-collapse specimens shown in Figures 14 and 15.

Because both specimens were subjected to the same applied hydraulic pressure under an equivalent test arrangement, the resulting deformation provides a direct comparative assessment of collapse morphology under the applied loading condition. Continuous load–displacement data were not recorded; consequently, the test does not quantify energy absorption or identify the load at which local buckling or tearing initiated.

Fig. 14. Tube specimens following compressive collapse under a 32-tonne hydraulic press. Both specimens were tested using the same applied hydraulic pressure and equivalent loading arrangement.

Fig. 15. Close-up comparison of the collapsed specimens. Visible tearing occurred in the 4130 Cr–Mo specimen within a region of severe local deformation. No comparable tearing or separation of the UltraTube RS longitudinal seam was observed under the applied loading condition. UltraTube RS is shown on the left.

7.3 Rotary Draw Bending Behaviour

Both materials were successfully formed using standard rotary draw tube-bending equipment without internal mandrel support, representing a fabrication condition commonly used in motorsport tube construction.

Fig. 16. Rotary draw tube-bending equipment used to form the nominal 38.1 mm tube specimens without internal mandrel support.

Table 2. Minimum post-bend diameter measurements for nominal 38.1 mm rotary-draw-bent tube specimens.

Material	Nominal outside diameter (mm)	Minimum post-bend diameter (mm)	Diameter reduction (%)
Seamless 4130 Cr-Mo tube	38.1	35.5	6.8
UltraTube RS dual-phase steel tube	38.1	36.1	5.2

As shown in Table 2, both specimens retained more than 90% of their original nominal outside diameter under the tested bending conditions. UltraTube RS exhibited a minimum post-bend diameter of 36.1 mm, corresponding to a diameter reduction of 5.2%, compared with 35.5 mm and 6.8%, respectively, for the seamless 4130 Cr–Mo specimen. The UltraTube RS result was also consistent with forming behaviour observed in additional bends undertaken during the product's development. These additional bends were not measured or included in the formal comparative dataset and are noted here as corroborating manufacturing experience.

Fig. 17. Rotary draw bending of nominal 38.1 mm tube specimens performed without internal mandrel support. UltraTube RS is shown at the top and seamless 4130 Cr–Mo tube at the bottom. Corresponding dimensional measurements are reported in Table 2.

7.4 Flattening Behaviour

Flattening tests were conducted as a qualitative comparative assessment of deformation behaviour under severe compressive loading. Both materials underwent substantial plastic deformation before exhibiting edge cracking and splitting.

The overall flattening response of the two materials was broadly comparable. However, the 4130 Cr–Mo specimen exhibited more pronounced cracking and greater edge separation in the final deformed condition.

The more pronounced cracking observed in the 4130 Cr–Mo specimen is consistent with its lower measured elongation and earlier tendency toward strain localisation identified during tensile testing. However, because the flattening assessment was qualitative and uninstrumented, the observed difference cannot be attributed conclusively to a specific material mechanism.

The tests were not instrumented, and no load–displacement, final-height or crack-length measurements were recorded. The results should therefore be interpreted as qualitative observations of deformation and final failure morphology rather than quantitative measures of forming limit or failure resistance.

Fig. 18. Flattened specimens following severe compressive deformation: (a) overall comparison of UltraTube RS and 4130 Cr–Mo specimens; (b) close-up of edge cracking in UltraTube RS; and (c) close-up of edge cracking and separation in 4130 Cr–Mo.

8. Discussion

The comparison undertaken in this study was designed to minimise the influence of nominal strength and section geometry. The tested materials exhibited closely comparable proof and ultimate tensile strengths, while the specimen dimensions and cross-sectional areas were effectively equivalent. Differences observed in the subsequent testing are therefore unlikely to be explained primarily by differences in nominal strength or section capacity. Instead, the results indicate differences in post-yield material response and, within welded joints, the local mechanical-property variation introduced by welding.

The tensile results provide the first indication of this distinction. UltraTube RS exhibited a lower yield-to-tensile strength ratio, greater total elongation and more distributed deformation within the reduced section before final localisation. The 4130 Cr–Mo specimen exhibited a higher yield ratio and more localised deformation. Total elongation alone does not describe how strain was distributed before fracture, because it includes deformation associated with necking and is influenced by specimen geometry and gauge length. However, when considered alongside the engineering stress–strain response and the photographed tensile specimens, the results indicate that UltraTube RS sustained post-yield deformation over a greater portion of the measured strain range before final localisation. This behaviour is consistent with the high initial strain-hardening response and low yield ratio commonly associated with dual-phase steels (ArcelorMittal, 2025; Huda, 2024).

The weld-zone hardness measurements identify a second important distinction. The 4130 Cr–Mo joint developed a pronounced local hardness increase from base-material values of approximately 266–306 HV to a peak of approximately 490 HV. This transition occurred over a comparatively narrow region of approximately 1–2 mm. UltraTube RS increased from base-material values of approximately 233–241 HV to a lower peak of approximately 312 HV, with a broader and more gradual transition through the HAZ and weld metal. The difference therefore lies not only in peak hardness but also in the magnitude and spatial gradient of the local property change.

A steep hardness gradient creates an abrupt transition between adjoining regions with different mechanical responses. Where such a transition occurs close to a geometric stress concentration, deformation may become concentrated within a relatively small material volume once yielding begins. Increased hardness is also generally associated with reduced local ductility and fracture toughness, although hardness alone does not provide a direct measurement of either property (Anderson, 2017; Dieter, 1986). The more gradual hardness transition measured in UltraTube RS is therefore consistent with a less abrupt local mechanical discontinuity, while the sharper transition measured in 4130 Cr–Mo provides conditions under which strain localisation may be more readily promoted. This interpretation concerns the measured weld-zone response and should not be taken as direct evidence of fracture resistance or fatigue life.

The finite element analysis provides the geometric context within which these weld-zone differences can be considered. Both material models developed their highest equivalent-stress demand around the

branch-to-main-tube interface, demonstrating that joint geometry primarily determines where stress concentration occurs. The broadly similar location of this demand in both models establishes a common geometric basis for comparison. Comparable global tensile strength did not remove the local stress concentration created by the branch-joint intersection.

The measured hardness gradients were not incorporated as spatial material properties within the finite element models, and the analysis did not include a damage or fracture criterion. It therefore does not calculate the direct effect of the HAZ hardness profiles or predict crack initiation. Nevertheless, the modelling and hardness measurements provide complementary information. In the 4130 Cr–Mo joint, the region of greatest geometric stress demand occurs in the same general area as a comparatively abrupt weld-zone hardness transition. In the UltraTube RS joint, the equivalent geometric demand occurs alongside a lower and more gradual measured hardness transition. The combined results suggest that the local mechanical environment within the critical joint region differs between the two materials, even though the location of peak geometric demand is broadly similar.

The fabrication trials demonstrated that both materials could be TIG welded successfully under representative motorsport workshop conditions. Macro examination of the two 77 A joints reported satisfactory penetration and complete fusion, with no cracks, slag or porosity observed in either specimen. The comparison should therefore not be interpreted as showing that one material could be welded successfully while the other could not. Rather, the significant distinction was the different hardness response produced across the resulting welded regions under the assessed conditions.

The physical deformation tests produced a mixture of common and differing outcomes. In three-point bending, both materials underwent substantial permanent deformation without visible fracture in the photographed specimens. In rotary draw bending, both nominal 38.1 mm specimens retained more than 90% of their original outside diameter. These results confirm that both materials were capable of accommodating the applied bending and forming conditions, but they do not establish a statistically significant difference in bending performance.

The clearest comparative difference was observed during axial compressive collapse. UltraTube RS developed broader and more progressive folding around the collapsed section, whereas 4130 Cr–Mo developed sharper, more localised folds and visible tearing within a region of severe deformation. No comparable tearing or separation of the UltraTube RS longitudinal production seam was observed under the applied loading condition. Because continuous load–displacement data were not recorded, the test does not quantify energy absorption or the load at which instability or tearing initiated. It does, however, provide a direct comparison of the final collapse morphology produced under an equivalent test arrangement.

Flattening produced broadly comparable overall deformation in both materials, with both specimens ultimately exhibiting edge cracking and splitting. More pronounced cracking and greater edge separation were visible in the 4130 Cr–Mo specimen. This observation is consistent with its lower measured elongation and earlier tendency toward strain localisation during tensile testing. However, the flattening test was qualitative and uninstrumented, and no final-height, crack-length or load–displacement measurements were recorded. The difference cannot therefore be attributed conclusively to a particular mechanism or used as a quantitative comparison of forming limit or failure resistance.

Taken together, the results do not demonstrate that either material is superior under every loading or fabrication condition. Both materials were successfully welded, bent and severely deformed under the conditions examined. The narrower and more defensible finding is that materials with closely comparable nominal tensile strength may nevertheless exhibit different post-yield responses and substantially different weld-zone hardness profiles. UltraTube RS exhibited characteristics consistent with more sustained strain accommodation and a more gradual local weld-zone transition, while 4130 Cr–Mo exhibited a higher yield ratio, a sharper HAZ hardness gradient and a greater tendency toward localised deformation in the compressive-collapse and qualitative flattening assessments.

These findings are particularly relevant to welded tubular structures because joint geometry determines where stress demand is concentrated, while material response and weld-induced property variation influence how deformation develops after yielding begins. Peak tensile strength alone is therefore insufficient to describe the local response of a welded tube assembly. Consideration should also be given to post-yield strain accommodation, weld-zone hardness gradients, joint geometry and the potential for deformation to become concentrated within a limited region.

The observed behaviour is also consistent with the established use of dual-phase steels in automotive body-in-white structures, where this material class is employed for its combination of high strength, formability and controlled deformation response (WorldAutoSteel, 2025). This widespread industrial adoption provides relevant context that dual-phase steel is a mature structural material system rather than an experimental alternative.

The present study does not directly measure crack-initiation resistance, fracture toughness, fatigue life or impact performance. It therefore cannot establish that one material will provide longer service life or greater resistance to fracture in a completed structure. It does, however, identify material and weld-zone characteristics that influence the conditions under which localised deformation may develop. In particular, the coincidence of geometric stress concentration with an abrupt local property transition provides a physically grounded basis for considering how crack initiation conditions may differ between welded tube material systems.

9. Limitations

This study provides a comparative assessment of the tested materials under the specific specimen geometries, welding conditions and loading arrangements examined. Although the materials were closely matched in strength and section profile, the number of specimens was limited, and the results do not establish the full statistical variation that may occur between production batches, tube dimensions or fabrication conditions.

Tensile testing was conducted in accordance with AS 1391:2020 and provides a quantitative comparison of proof strength, ultimate tensile strength and elongation after fracture. However, elongation is influenced by specimen geometry, gauge length and post-necking deformation and should therefore be interpreted alongside the measured stress–strain response and observed deformation morphology rather than as a standalone indicator of structural performance. The three-point bending, compressive-collapse and flattening assessments were comparative workshop tests rather than standardised mechanical test methods. With the exception of the reported rotary-draw-bending dimensions, these assessments were based primarily on observed deformation morphology. They do not provide quantitative measures of absorbed energy, collapse resistance, fracture resistance or structural capacity.

The weld-zone hardness results apply to the tested TIG-welded branch joints and may vary with welding current, heat input, joint geometry, filler material and fabrication practice. Hardness provides evidence of local mechanical-property variation but does not directly measure ductility, fracture toughness, residual stress or fatigue performance. Metallographic phase identification was not undertaken to confirm the precise microstructures responsible for the measured hardness profiles.

The finite element analysis identified the location and distribution of geometric stress demand using parent-material models derived from the measured stress–strain curves. The measured weld-zone hardness distributions were not incorporated as spatial material properties, and the models did not include damage or fracture criteria. The analysis should therefore not be interpreted as a direct prediction of crack initiation, fracture or fatigue life.

Fatigue, repeated cyclic loading, impact behaviour, fracture toughness and long-term structural durability were not measured directly. The findings should therefore be interpreted as comparative evidence of material, weld-zone and deformation behaviour under the conditions tested, rather than as design allowables or qualification of either material for a particular structure.

10. Conclusions

This study compared seamless normalised AISI 4130 Cr–Mo tube with UltraTube RS dual-phase HFIW tube under conditions in which tensile strength and section geometry were closely matched. The results demonstrate that materials with comparable nominal strength can nevertheless exhibit materially different post-yield responses and weld-zone mechanical-property distributions.

Tensile testing showed closely comparable proof and ultimate tensile strengths. UltraTube RS exhibited a lower yield-to-tensile strength ratio, greater elongation and deformation distributed over a greater portion of the tensile specimen before final localisation. The 4130 Cr–Mo specimen exhibited a higher yield ratio and a more localised final deformation response. These findings indicate that the principal tensile distinction between the materials lies in their behaviour after yielding rather than in peak strength alone.

Both materials were successfully TIG welded into representative branch joints under comparable

workshop conditions, with satisfactory penetration and complete fusion reported in both 77 A specimens. However, the resulting weld-zone hardness profiles differed substantially. The 4130 Cr–Mo joint developed a pronounced local HAZ peak of approximately 490 HV and a steep property transition over a narrow region. UltraTube RS developed a lower peak of approximately 312 HV and a broader, more gradual transition across the weld region.

Finite element analysis identified the branch-to-main-tube interface as the principal region of geometric stress demand for both material models. This confirms that joint geometry largely determines where stress becomes concentrated. When considered alongside the hardness measurements, the results show that equivalent geometric demand can occur within substantially different local mechanical environments. In the tested 4130 Cr–Mo joint, the critical geometric region coincided with a comparatively abrupt weld-zone hardness transition, whereas the UltraTube RS joint exhibited a lower and more gradual transition in the same general region. The analysis did not directly model the measured hardness gradients or predict fracture.

The physical testing demonstrated that both materials could accommodate severe deformation under the applied conditions. Both specimens underwent substantial permanent deformation without visible fracture during three-point bending, and both retained more than 90% of their nominal outside diameter during rotary draw bending. These results confirm satisfactory forming behaviour for both materials under the tested arrangements rather than establishing a clear comparative advantage in bending performance.

The clearest difference in tube-level deformation occurred during axial compressive collapse. UltraTube RS developed broader and more progressive folding, whereas the 4130 Cr–Mo specimen developed sharper localised folds and visible tearing within a region of severe deformation. No comparable tearing or separation of the UltraTube RS longitudinal production seam was observed. During qualitative flattening, both materials exhibited edge cracking and splitting, although greater crack opening and edge separation were visible in the 4130 Cr–Mo specimen. Because these tests were not fully instrumented, the observations describe deformation morphology and do not quantify energy absorption, fracture resistance or structural capacity.

Taken together, the findings indicate that the distinction between the tested materials cannot be described by tensile strength alone. UltraTube RS exhibited a post-yield response consistent with more sustained strain accommodation and developed a less abrupt weld-zone hardness transition. The tested 4130 Cr–Mo material exhibited a greater tendency toward localised deformation in the tensile and compressive-collapse assessments and developed a markedly sharper hardness gradient adjacent to the weld.

These characteristics are relevant in welded tubular structures because joint geometry establishes where stress demand occurs, while the local material and weld-zone response influences how deformation develops once yielding begins. Material selection should therefore consider post-yield behaviour, weld-zone property variation, fabrication conditions and joint geometry alongside conventional proof and ultimate tensile strength.

This study did not directly measure fracture toughness, fatigue life, repeated-load performance or long-term durability. The findings should therefore be interpreted as a comparative assessment of the tested materials and welded joints under the specified conditions, rather than as structural qualification or evidence of service life for a particular application.

---

11. Author Disclosure

UltraTube RS is a dual-phase steel tube product manufactured by Industrial Tube Manufacturing. The author is involved in the development and supply of this material. All formal testing presented in this study was conducted by independent third-party laboratories, and the results are reported as received. Test specimens were prepared using standard production material and processes representative of commercial supply.

---

12. Technical Disclaimer

The information presented in this study is believed to be accurate within the scope of the testing described. It is provided for technical and comparative information only and does not constitute design approval, engineering certification or a recommendation that either material is suitable for a particular structure or application. Material selection, joint design, fabrication procedures and structural validation remain the responsibility of the relevant designer, fabricator and approving authority.

13. Acknowledgements

The author gratefully acknowledges Luis Rodrigo Palomera, MSc in Advanced Technology, Metallurgist Technical Representative at Tata Steel Europe, for his independent technical review of the manuscript and for his comments on advanced high-strength steels, automotive metallurgy, and the interpretation of the study findings.

The author also acknowledges Vladimir Stojanovic, MEng (Metallurgy), BEng, IWE, Metallurgist at Materials & Testing Laboratories, for his detailed technical review and comments, which contributed to improvements in the technical accuracy and clarity of the manuscript.

The author further acknowledges Materials & Testing Laboratories, Auckland, for conducting the independent tensile testing, micro-Vickers hardness testing and metallurgical assessment, and Kinetic Simulation for undertaking the finite element modelling and associated engineering analysis.

References

SAE International (2023). *SAE AMS6360R: Steel Mechanical Tubing, Seamless, 0.95Cr–0.20Mo (0.28–0.33C) (4130), Aircraft Quality, Normalized and Tempered, or Stress Relieved*. Warrendale, PA: SAE International. https://doi.org/10.4271/AMS6360R

Fonstein, N. (2015). *Advanced High Strength Sheet Steels: Physical Metallurgy, Design, Processing, and Properties*. Cham: Springer. https://doi.org/10.1007/978-3-319-19165-2

WorldAutoSteel (2025). *Advanced High-Strength Steel Application Guidelines*. Brussels: World Steel Association. Available at: https://ahssinsights.org/ (Accessed: 7 August 2026).

ASM International (1998). *'Steel tubular products', in Davis, J.R. (ed.) Metals Handbook Desk Edition.* 2nd ed. Materials Park, OH: ASM International, pp. 242–244. doi: 10.31399/asm.hb.mhde2.a0003096.

Dieter, G.E. (1986). *Mechanical Metallurgy*. 3rd ed. New York: McGraw-Hill.

Bhadeshia, H.K.D.H. and Honeycombe, R.W.K. (2017). *Steels: Microstructure and Properties*. 4th ed. Oxford: Butterworth-Heinemann.

ArcelorMittal (2025). *Dual Phase Steels. North American Automotive Product Data Sheet*. Available at: https://northamerica.arcelormittal.com/media/2aenqa2s/arcelormittal_data-sheet_dual-phase-steels_2025_x1a.pdf (Accessed: 7 August 2026).

Kou, S. (2003). *Welding Metallurgy*. 2nd ed. Hoboken, NJ: John Wiley & Sons. https://doi.org/10.1002/0471434027

ASM International (2011). *ASM Handbook, Volume 6A: Welding Fundamentals and Processes*. Materials Park, OH: ASM International.

Cao, Y., Ahlström, J. and Karlsson, B. (2015). 'The influence of temperatures and strain rates on the mechanical behavior of dual phase steel in different conditions', *Journal of Materials Research and Technology*, *4*(1), pp. 68–74. https://doi.org/10.1016/j.jmrt.2014.11.001

Standards Australia (2020). *AS 1391:2020 Metallic Materials—Tensile Testing—Method of Test at Room Temperature*. Sydney: Standards Australia.

International Organization for Standardization (2019). *ISO 6892-1:2019 Metallic Materials—Tensile Testing—Part 1: Method of Test at Room Temperature*. Geneva: ISO.

Materials & Testing Laboratories (2026c). *Tensile Test Report: 4130 Cr–Mo Tube Specimen*. Report No. J69467.1. Auckland: Materials & Testing Laboratories.

Materials & Testing Laboratories (2026d). *Tensile Test Report: UltraTube RS Tube Specimen*. Report No. J69467.2. Auckland: Materials & Testing Laboratories.

Huda, Z. (2024). *Metal Forming Processes: Fundamentals, Analysis, Calculations*. Cham: Springer. https://doi.org/10.1007/978-3-031-56760-5

SSAB (n.d.). *The Forming Myth: Why Elongation Is Not a Good Measure of Formability When It Comes to Advanced High Strength Steel*. Available at: https:/www.ssab.com/en/brands-and-products/ssab-docol/automotive-steel-resources/automotive-insights/the-forming-myth (Accessed: 7 August 2026).

Materials & Testing Laboratories (2026a). *Macro and Micro-Vickers Hardness Test Report: UltraTube RS TIG Welded Joint (77 A Sample)*. Report No. J69467.4. Auckland: Materials & Testing Laboratories.

Materials & Testing Laboratories (2026b). *Macro and Micro-Vickers Hardness Test Report: 4130 Cr–Mo TIG Welded Joint (77 A Sample)*. Report No. J69467.3. Auckland: Materials & Testing Laboratories.

Kou, S. (2003). *Welding Metallurgy*. 2nd ed. Hoboken, NJ: John Wiley & Sons. https://doi.org/10.1002/0471434027

Farabi, N., Chen, D.L. and Zhou, Y. (2010). 'Fatigue properties of laser welded dual-phase steel joints', *Procedia Engineering*, *2*(1), pp. 835–843. https://doi.org/10.1016/j.proeng.2010.03.090

Lee, J.H., Park, S.H., Kwon, H.S., Kim, G.S. and Lee, C.S. (2014). 'Laser, tungsten inert gas, and metal active gas welding of DP780 steel: Comparison of hardness, tensile properties and fatigue resistance', *Materials & Design*, *64*, pp. 559–565. https://doi.org/10.1016/j.matdes.2014.07.065

Xie, L., Shi, B., Xiao, Z., Ren, J. and Li, D. (2021). 'Fatigue characteristics of DP780 steel spot welding joints with different static fracture modes', *Materials Transactions*, *62*(2), pp. 191–197. https://doi.org/10.2320/matertrans.MT-M2020214

Anderson, T.L. (2017). *Fracture Mechanics: Fundamentals and Applications.* 4th ed. Boca Raton, FL: CRC Press.

Kinetic Simulation (2026). *Comparative Finite Element Analysis of Welded Branch Joints: 4130 Cr–Mo and UltraTube RS*. Unpublished technical report prepared for Industrial Tube Manufacturing.

Shao, Y.B. (2007). 'Geometrical effect on the stress distribution along weld toe for tubular T- and K-joints under axial loading', *Journal of Constructional Steel Research*, *63*(10), pp. 1351–1360. https://doi.org/10.1016/j.jcsr.2006.12.005

Peng, Y., Wu, C., Gan, J. and Dong, J. (2018). 'Determination of the local constitutive properties of the welded steel joints using digital image correlation method', *Construction and Building Materials*, *171*, pp. 485–492. https://doi.org/10.1016/j.conbuildmat.2018.03.182

Appendix A – Macro and Micro Vickers Hardness Test Reports

Materials & Testing Laboratories (MTL) reports J69467.3 and J69467.4 are reproduced in full.

MTL Materials & Testing Laboratories

MACRO AND MICRO-VICKERS HARDNESS TEST REPORT

MTL Report No: J69467.4 **Date Tested:** 4 March, 2026

ADMINISTRATIVE AND CLIENT DETAILS			
Client Name:	Industrial Tube Manufacturing	**Attention:**	Jared Knapp
Purchase Order No:	Jared	**Contact Details:**	jared.knapp@industrialtube.co.nz
Testing Technician:	Sheik Mahaboob Raja | B.E. MatSciEng | Pg.Dip. MatSci		
Job Description:	Macro Examination		
SAMPLE IDENTIFICATION			
Test Method Standard:	NA	**Acceptance Criteria:**	Report findings
Joint Type:	Branch tube weld		
Material:	Ultra tube RS 1	**Material Thickness (mm):**	1.6 WT
Welding Procedure:	Not specified	**Welding Process:**	TIG
Marking:	77-amp samples	**Welder ID:**	Not specified
PREPARATION			
Etching Method:	Chemical etching	**Magnification:**	Up To 10X
Etchant Used:	5% Nital Acid	**Object Examined:**	Weld Metal

MICRO EXAMINATION RESULTS

Observations:	
Cracks	NIL
Slag	NIL
Porosity	NIL
Penetration	Satisfactory
Fusion	Complete fusion
Comments	NA

Image.1. Macro -1

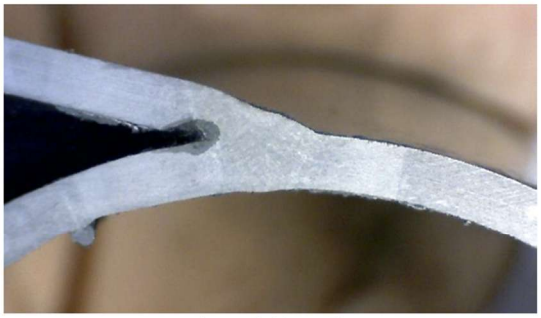

Image.2. Macro -2

This report must only be re-printed in full. This document is issued by the Company under its Terms and Conditions. Any unauthorized alteration, forgery or falsification of the content or appearance of this document is unlawful, and offenders may be prosecuted to the fullest extent of the law. Information on the report supplied by the customer may affect validity of results. Unless otherwise stated the results shown in this test report refer only to the sample(s) as received and tested.

MTL Materials & Testing Laboratories

MACRO AND MICRO-VICKERS HARDNESS TEST REPORT

MICRO-VICKERS HARDNESS TEST	
Test Method:	NA
Testing Equipment:	Micro Vickers hardness tester – Matsuzawa| Model No: (MHT-1, No: 8795) |
Test Surface:	Core
Test Temperature (°C):	23
Sample Identification:	TIG Ultra tube RS 1, 77-amp sample
Material:	Ultra tube RS 1

RESULTS

Micro-Vickers Diamond Pyramid Hardness values with 0.5kg load as shown below.

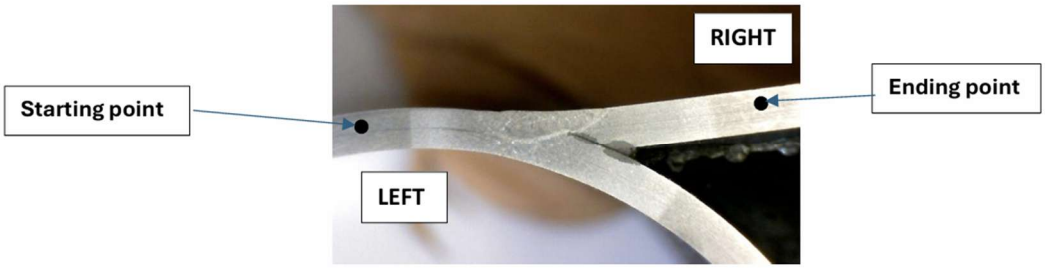

SL NO	Location	Spacing between indentations (mm)	HV 0.5kg	SL NO	Location	Spacing between indentations (mm)	HV 0.5kg
1	Base	0	241	18	HAZ	8.5	219
2	Base	0.5	234	19	Weld	9.0	296
3	Base	1.0	239	20	Weld	9.5	285
4	Base	1.5	234	21	Weld	10	297
5	Base	2.0	233	22	Weld	10.5	303
6	Base	2.5	235	23	Weld	11	286
7	Base	3.0	241	24	Weld	11.5	241
8	HAZ	3.5	234	25	HAZ	12	226
9	HAZ	4.0	219	26	HAZ	12.5	223
10	HAZ	4.5	276	27	HAZ	13	234
11	HAZ	5.0	312	28	HAZ	13.5	210
12	HAZ	5.5	290	29	HAZ	14	212
13	HAZ	6.0	294	30	HAZ	14.5	216
14	Weld	6.5	306	31	Base	15	218
15	Weld	7.0	293	32	Base	15.5	217
16	Weld	7.5	295	33	Base	16	220
17	Weld	8.0	306				

Note: Hardness measurements were carried out from left to right with 0.5 mm spacing. The starting and ending points are indicated in the image above for illustrative purposes.

This report must only be re-printed in full. This document is issued by the Company under its Terms and Conditions. Any unauthorized alteration, forgery or falsification of the content or appearance of this document is unlawful, and offenders may be prosecuted to the fullest extent of the law. Information on the report supplied by the customer may affect validity of results. Unless otherwise stated the results shown in this test report refer only to the sample(s) as received and tested.

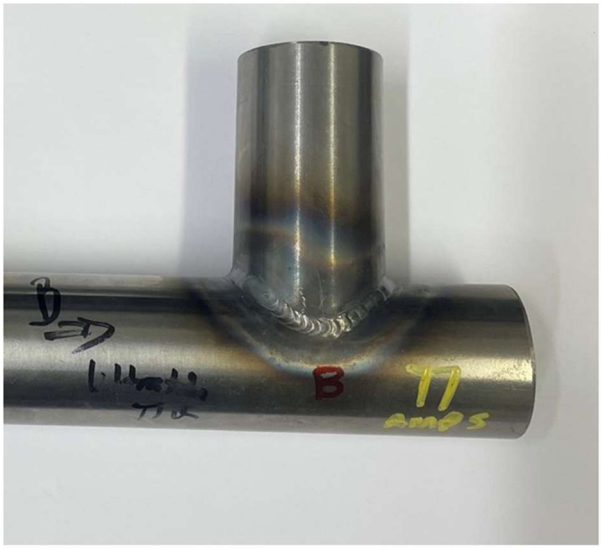

Image.3 As received sample

REVIEWAL AND APPROVAL			
There were no deviations or departures from the mentioned standards.			
Date of Review:	5 March, 2026	**Issue Date:**	5 March, 2026
Reviewed By:	Rex Ong	**Key Technical Person:**	Sheik Mahaboob Raja
Qualification:	B.Sci | Pg.Dip	**Qualification:**	B.E. MatSciEng | Pg.Dip. MatSci
Signature:		**Signature:**	

This report must only be re-printed in full. This document is issued by the Company under its Terms and Conditions. Any unauthorized alteration, forgery or falsification of the content or appearance of this document is unlawful, and offenders may be prosecuted to the fullest extent of the law. Information on the report supplied by the customer may affect validity of results. Unless otherwise stated the results shown in this test report refer only to the sample(s) as received and tested.

MTL Materials & Testing Laboratories

MACRO AND MICRO-VICKERS HARDNESS TEST REPORT

MTL Report No: J69467.3 **Date Tested:** 5 March, 2026

ADMINISTRATIVE AND CLIENT DETAILS			
Client Name:	Industrial Tube Manufacturing	**Attention:**	Jared Knapp
Purchase Order No:		**Contact Details:**	jared.knapp@industrialtube.co.nz
Testing Technician:	Sheik Mahaboob Raja | B.E. MatSciEng | Pg.Dip. MatSci		
Job Description:	Macro Examination		
SAMPLE IDENTIFICATION			
Test Method Standard:	NA	**Acceptance Criteria:**	Report findings
Joint Type:	Branch tube weld		
Material:	4130 chromoly	**Material Thickness (mm):**	1.6 WT
Welding Procedure:	Not specified	**Welding Process:**	TIG
Marking:	77-amp samples	**Welder ID:**	Not specified
PREPARATION			
Etching Method:	Chemical etching	**Magnification:**	Up To 10X
Etchant Used:	5% Nital Acid	**Object Examined:**	Weld Metal

MICRO EXAMINATION RESULTS

Observations:	
Cracks	NIL
Slag	NIL
Porosity	NIL
Penetration	Satisfactory
Fusion	Complete fusion
Comments	NA

Image.1. Macro -1

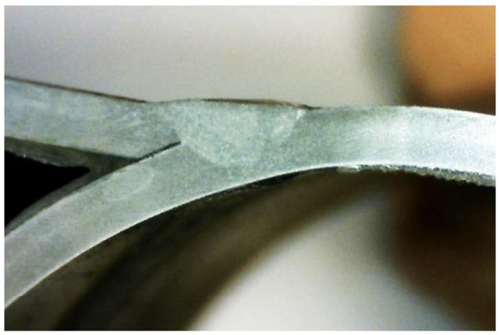

Image.2. Macro -2

This report must only be re-printed in full. This document is issued by the Company under its Terms and Conditions. Any unauthorized alteration, forgery or falsification of the content or appearance of this document is unlawful, and offenders may be prosecuted to the fullest extent of the law. Information on the report supplied by the customer may affect validity of results. Unless otherwise stated the results shown in this test report refer only to the sample(s) as received and tested.

MTL Materials & Testing Laboratories

MACRO AND MICRO-VICKERS HARDNESS TEST REPORT

MICRO-VICKERS HARDNESS TEST	
Test Method:	NA
Testing Equipment:	Micro Vickers hardness tester – Matsuzawa| Model No: (MHT-1, No: 8795) |
Test Surface:	Core
Test Temperature (°C):	23
Sample Identification:	TIG 4130, 77-amp sample
Material:	4130 Chromoly

RESULTS

Micro-Vickers Diamond Pyramid Hardness values with 0.5kg load as shown below.

SL NO	Location	Spacing between indentations (mm)	HV 0.5kg	SL NO	Location	Spacing between indentations (mm)	HV 0.5kg
1	Base	0	274	16	Weld	7.5	432
2	Base	0.5	266	17	Weld	8	422
3	Base	1.0	267	18	Weld	8.5	402
4	Base	1.5	280	19	Weld	9	394
5	Base	2.0	285	20	Weld	9.5	392
6	Base	2.5	281	21	HAZ	10	490
7	Base	3.0	306	22	HAZ	10.5	468
8	HAZ	3.5	356	23	HAZ	11	458
9	HAZ	4.0	402	24	HAZ	11.5	429
10	HAZ	4.5	490	25	Base	12	306
11	HAZ	5.0	438	26	Base	12.5	301
12	HAZ	5.5	456	27	Base	13	266
13	HAZ	6.0	429	28	Base	13.5	271
14	Weld	6.5	419	29	Base	14	285
15	Weld	7.0	428				

Note: Hardness measurements were carried out from left to right with 0.5 mm spacing. The starting and ending points are indicated in the image above for illustrative purposes.

This report must only be re-printed in full. This document is issued by the Company under its Terms and Conditions. Any unauthorized alteration, forgery or falsification of the content or appearance of this document is unlawful, and offenders may be prosecuted to the fullest extent of the law. Information on the report supplied by the customer may affect validity of results. Unless otherwise stated the results shown in this test report refer only to the sample(s) as received and tested.

Image.3 As received sample.

REVIEWAL AND APPROVAL			
There were no deviations or departures from the mentioned standards.			
Date of Review:	5 March, 2026	**Issue Date:**	5 March, 2026
Reviewed By:	Rex Ong	**Key Technical Person:**	Sheik Mahaboob Raja
Qualification:	B.Sci | Pg.Dip	**Qualification:**	B.E. MatSciEng | Pg.Dip. MatSci
Signature:		**Signature:**	

This report must only be re-printed in full. This document is issued by the Company under its Terms and Conditions. Any unauthorized alteration, forgery or falsification of the content or appearance of this document is unlawful, and offenders may be prosecuted to the fullest extent of the law. Information on the report supplied by the customer may affect validity of results. Unless otherwise stated the results shown in this test report refer only to the sample(s) as received and tested.

Appendix B – Tensile Test Reports

Materials & Testing Laboratories (MTL) reports J69467.1 and J69467.2 are reproduced in full.

MTL Materials & Testing Laboratories

TENSILE TEST REPORT

ACCREDITED IANZ TESTING LABORATORY

All tests reported herein have been performed in accordance with the laboratory's scope of accreditation

MTL Report No: J69467.2 **Date Tested:** 3 March, 2026

ADMINISTRATIVE AND CLIENT DETAILS			
Client Name:	Industrial Tube Manufacturing	**Attention:**	Jared Knapp
Purchase Order No:	Jared	**Contact Details:**	jared.knapp@industrialtube.co.nz
Testing Technician:	Rex Ong | B.Sci | Pg.Dip		
Job Description:	Tensile 0.2% Proof Testing on Supplied Samples		

TENSILE TEST			
Test Method Standard:	AS 1391 : 2020		
Testing Equipment:	Shimadzu Universal Grade 1 Testing Machine | Model No: UH 500 KNI | SN NM: 121054600016		
Specimen Orientation:	Longitudinal	**Aging:**	None

RESULTS	
Test Number:	**1**
Sample Identification:	TIG Ultra Tube RS 1.65 x 38.1
Heat Number:	Not Supplied
Diameter / Dimensions (mm):	1.61 x 12.51
Area (mm^2):	20.1
Gauge Length (mm):	50
0.2% Proof Load (kN):	14.4
0.2% Proof Strength (MPa):	713
Ultimate Tensile Load (kN):	17.4
Ultimate Tensile Strength (MPa):	862
Elongation after Fracture (%):	19.5
Notes:	

REVIEWAL AND APPROVAL			
There were no deviations or departures from the mentioned standards.			
Date of Review:	3 March, 2026	**Issue Date:**	3 March, 2026
Reviewed By:	Vladimir Stojanovic	**Key Technical Person:**	Rex Ong
Qualification:	B.E. Met | M.Eng Met	**Qualification:**	B.Sci | Pg.Dip
Signature:		**Signature:**	

This report must only be re-printed in full. This document is issued by the Company under its Terms and Conditions. Any unauthorized alteration, forgery or falsification of the content or appearance of this document is unlawful, and offenders may be prosecuted to the fullest extent of the law. Information on the report supplied by the customer may affect validity of results. Unless otherwise stated the results shown in this test report refer only to the sample(s) as received and tested.

MTL Materials & Testing Laboratories

TENSILE TEST REPORT

ACCREDITED IANZ TESTING LABORATORY

All tests reported herein have been performed in accordance with the laboratory's scope of accreditation

MTL Report No: J69467.1 **Date Tested:** 3 March, 2026

ADMINISTRATIVE AND CLIENT DETAILS			
Client Name:	Industrial Tube Manufacturing	**Attention:**	Jared Knapp
Purchase Order No:	Jared	**Contact Details:**	jared.knapp@industrialtube.co.nz
Testing Technician:	Rex Ong | B.Sci | Pg.Dip		
Job Description:	Tensile 0.2% Proof Testing on Supplied Samples		

TENSILE TEST			
Test Method Standard:	AS 1391 : 2020		
Testing Equipment:	Shimadzu Universal Grade 1 Testing Machine | Model No: UH 500 KNI | SN NM: 121054600016		
Specimen Orientation:	Longitudinal	**Aging:**	None

RESULTS	
Test Number:	**1**
Sample Identification:	TIG 4130 Chromoly 1.65 x 38.1
Heat Number:	Not Supplied
Diameter / Dimensions (mm):	1.65 x 12.50
Area (mm²):	20.6
Gauge Length (mm):	50
0.2% Proof Load (kN):	15.1
0.2% Proof Strength (MPa):	732
Ultimate Tensile Load (kN):	17.8
Ultimate Tensile Strength (MPa):	863
Elongation after Fracture (%):	13.8
Notes:	

REVIEWAL AND APPROVAL			
There were no deviations or departures from the mentioned standards.			
Date of Review:	3 March, 2026	**Issue Date:**	3 March, 2026
Reviewed By:	Vladimir Stojanovic	**Key Technical Person:**	Rex Ong
Qualification:	B.E. Met | M.Eng Met	**Qualification:**	B.Sci | Pg.Dip
Signature:		**Signature:**	

This report must only be re-printed in full. This document is issued by the Company under its Terms and Conditions. Any unauthorized alteration, forgery or falsification of the content or appearance of this document is unlawful, and offenders may be prosecuted to the fullest extent of the law. Information on the report supplied by the customer may affect validity of results. Unless otherwise stated the results shown in this test report refer only to the sample(s) as received and tested.